Research Square

Preprints are preliminary reports that have not undergone peer review.
They should not be considered conclusive, used to inform clinical practice,
or referenced by the media as validated information.

Single-cell RNA sequencing of brain tissue from a mouse model of phenylketonuria

Huimin Gao

184035505840163.com

Capital Medical University Beijing Obstetrics and Gynecology Hospital https://orcid.org/0009-0004-8874-6022

Wenxiang Liu

Capital Medical University Beijing Obstetrics and Gynecology Hospital

Chuan Zhang

Gansu Provincial Cancer Hospital

Xiaohua Jin

Gansu Provincial Cancer Hospital

Wei Zhong

Capital Medical University Beijing Obstetrics and Gynecology Hospital

Yanhong Zhai

Beijing Maternal and Child Health Care Hospital: Capital Medical University Beijing Obstetrics and Gynecology Hospital

Zhengyang Yao

Capital Medical University Beijing Obstetrics and Gynecology Hospital

Huihui Yan

Capital Medical University Beijing Obstetrics and Gynecology Hospital

Wenjing Hao

Capital Medical University Beijing Obstetrics and Gynecology Hospital

Yu Wang

National Research Institute for Family Planning

Xiaofang Cao

National Research Institute for Family Planning

Zheng Cao

Capital Medical University Beijing Obstetrics and Gynecology Hospital

Yousheng Yan

Capital Medical University Beijing Obstetrics and Gynecology Hospital

Chenghong Yin

Capital Medical University Beijing Obstetrics and Gynecology Hospital

Research Article

Keywords: Phenylketonuria, Single-cell RNA sequencing, Neuroinflammation, Synaptic dysfunction, Cellular stress

Posted Date: March 11th, 2026

DOI: https://doi.org/10.21203/rs.3.rs-8406037/v1

License: This work is licensed under a Creative Commons Attribution 4.0 International License. Read Full License

---

Version of Record: A version of this preprint was published at Orphanet Journal of Rare Diseases on November 15th, 2026. See the published version at https://doi.org/10.1186/s13023-026-04613-x.

Abstract

Phenylketonuria (PKU), the most common inherited metabolic disorder, results from PAH mutations causing hyperphenylalaninemia and brain injury. While low-phenylalanine dietary therapy alleviates neurological symptoms, brain damage mechanisms remain unclear. Using our established PKU mouse model, we performed single-cell RNA sequencing of 38,678 brain cells to elucidate the cellular and molecular mechanisms underlying PKU-associated brain dysfunction. We identified widespread transcriptomic alterations across neuronal, glial, and immune compartments. Microglia and astrocytes exhibited elevated expression of oxidative stress and neuroinflammation genes, implicating neurotoxic roles. Neuronal populations displayed dysregulated synaptic transmission and plasticity genes, potentially contributing to cognitive impairments in PKU. Additionally, altered blood–brain barrier and cerebrovascular gene expression suggested vascular pathology contributes to brain injury. Our findings provide the first comprehensive cellular and molecular map of the PKU-affected brain, offering fresh insights into its complex pathophysiology and guiding development of specific therapeutics beyond dietary management.

1. Introduction

Phenylketonuria (PKU) is a widespread hereditary metabolic condition that occurs in approximately 1 in 10,000 to 15,000 live births globally.[1] This condition results from mutations in the gene encoding phenylalanine hydroxylase (PAH) that result in a deficit of the enzyme that converts phenylalanine (PHE) into tyrosine.[2] Consequently, there is excessive PHE accumulation in the blood and brain, especially during early embryonic phases.[3] This metabolic disorder is extremely neurotoxic and, if ignored, leads to substantial cognitive impairments, behavioral abnormalities, seizures, and many neurological issues.

The timely identification by newborn screening and the enforcement of a stringent low-PHE diet have greatly enhanced the clinical outlook for individuals with PKU. Nonetheless, despite continuous nutritional adjustments, a relatively large proportion of patients demonstrate minor but enduring abnormalities in executive function, attention, motor coordination, and emotional regulation.[4] This indicates that elevated PHE levels may have enduring effects on neurodevelopment and cerebral function that are not entirely reversible by dietary modification.[5] The fundamental mechanisms underlying these effects remain inadequately understood, which presents an important obstacle to the development of supplementary or alternative treatment procedures.

Prior studies in human subjects and animal models have identified various anatomical and functional cerebral alterations that are associated with PKU, encompassing white matter degeneration, impaired myelination, modified neurotransmitter concentrations, and glial activation.[3, 6, 7] However, the majority of these investigations have depended on bulk tissue analyses or low-resolution techniques, which may mask transcriptional alterations unique to different cell types. Although a recent study has applied scRNA-seq to the corpus callosum of the classic Pah^enu2 PKU mouse model,[8] a brain-wide understanding of how diverse cell populations respond to hyperphenylalaninemia, particularly in a model

that more accurately recapitulates a human-specific splicing defect, remains to be elucidated. This restricts our mechanistic understanding of the cellular foundations of PKU neuropathology.

Given the complex cellular structure of the brain, a high-resolution methodology is essential for elucidating the responses of various brain cell types to chronic metabolic stress in PKU. In this setting, single-cell RNA sequencing (scRNA-seq) has emerged as a potent method for elucidating the transcriptional profile of individual cells inside complex tissues. This technology facilitates the impartial identification of unique neural and glial populations and reveals cell-type-specific modifications in gene expression, signaling pathways, and cellular states.

This study aimed to utilize scRNA-seq in a PKU mouse model to uncover cell type-specific molecular mechanisms underlying PKU-associated brain dysfunction. Addressing the limitations of prior bulk-tissue analyses, we focused on dissecting distinct transcriptomic responses to chronic hyperphenylalaninemia stress in neurons, glial cells, and endothelial cells. By identifying key differentially expressed genes and enriched pathways, we sought to elucidate how elevated phenylalanine disrupts neurovascular homeostasis, induces neuroinflammation/oxidative stress, and impairs synaptic function. These findings may inform the development of specific therapies designed to reduce neurological damage and enhance outcomes for individuals with PKU.

2. Materials and methods

2.1 Model mice

The present study strictly complied with all pertinent ethical rules for mouse breeding, testing, and research. The animal trials received approval from the Ethics Committee of Beijing Obstetrics and Gynecology Hospital, Capital Medical University (Approval No. BOGH21-2404-3). All mouse experiments were conducted in stringent compliance with the directives of the Animal Experiment Management Committee. All experimental procedures were performed by certified personnel trained in laboratory animal handling. Mice were maintained under standardized housing conditions, including a controlled temperature (22 ~ 25℃) and humidity (45%~60%), a 12-hour light/dark cycle, dry bedding, sufficient ventilation, and *ad libitum* access to food and water.

The mice used in this study were of the C57BL/6J strain and were obtained from Shanghai Model Organisms Center, Inc. Using CRISPR/Cas9-mediated genome editing combined with homologous recombination, we generated a partially humanized *PAH* knock-in mouse model. Specifically, human *PAH* exons 11–12, harboring either the c.1199 + 502A > T variant or the corresponding WT (c.1199 + 502WT) sequence, were inserted into the endogenous *Pah* gene locus. This approach allowed us to reproduce the deleterious phenotypic effects of poor responsiveness, body weakness, and yellowing of the fur associated with the variant, and to develop a homozygous PKU model mouse with a partially humanized Pah gene.

To ensure genetic stability, F1 generation mice were continuously backcrossed with WT C57BL/6J mice for 10 generations. Homozygous mice carrying either mutant (c.1199 + 502A > T) or WT (c.1199 + 502WT) alleles were obtained by intercrossing heterozygous mice and were used in subsequent experiments. All animals used in this study were 8-week-old male mice.

2.2 Mice brain tissue dissection

Mice underwent carbon dioxide anesthesia followed by cervical dislocation in accordance with institutional animal care guidelines. The skull was then carefully opened and the whole brain was rapidly extracted. Dissected brain tissue was immediately transferred into a 15 mL centrifuge tube containing ice-cold calcium- and magnesium-free Dulbecco's phosphate-buffered saline to preserve tissue integrity for downstream processing.

2.3 Single-cell suspension preparation

Brain tissue was washed twice under sterile conditions with pre-chilled RPMI 1640 medium containing 0.04% bovine serum albumin before being minced into approximately 0.5 mm^3 pieces. The tissue pieces were then enzymatically digested in 1 mg/mL collagenase I and 0.5 mg/mL DNase I at 37°C with 250 rpm agitation for 1 hour. The resulting suspension was filtered through a 40 μm cell strainer and centrifuged at 300 × *g* for 5 minutes at 4°C.

Next, the pellet was resuspended in culture medium and treated with an equal volume of red blood cell lysis buffer (MACS, #130-094-183) at 4°C for 10 minutes. Following centrifugation, cells were washed once, pelleted again, and finally resuspended in 100 μL of growth medium. Cell viability and concentration were assessed using a Luna cell counter.

2.4 scRNA-seq library preparation and sequencing

The newly manufactured single-cell suspension was calibrated to a concentration of 700–1200 cells/μL. Library building was executed in accordance with the guidelines specified in the 10× Genomics Chromium Next GEM Single Cell 3' Reagent Kits v3.1 (catalog number: 1000268). The assembled libraries were subsequently sequenced on the Illumina NovaSeq 6000 platform using the PE150 sequencing protocol. Cell preparation and single-cell sequencing were performed using the MobiNova-100 platform (MobiDrop, Zhejiang, China) by OE Biotech Co., Ltd. (Shanghai, China), following the manufacturer's instructions.

2.5 scRNA-seq data preprocessing

Raw sequencing data in FASTQ format were aligned to the mm10 mouse reference genome using Cell Ranger software (version 8.0.1) from 10× Genomics. This technique entailed consolidating the unique molecular identifier (UMI) numbers for each barcode to produce a UMI count matrix. Subsequent analysis was conducted using Seurat R (version 4.0.0).

2.6 Quality control and filtering

To ensure data integrity, stringent quality control measures were applied to remove low-quality cells and potential doublets. Cells with < 200 detected genes, total UMI counts < 1,000, or $\log_{10}$GenesPerUMI values < 0.7 were excluded. Additionally, cells with > 10% of UMIs mapped to mitochondrial genes or > 5% of UMIs mapped to hemoglobin genes were removed. Probable doublets were identified and eliminated using the DoubletFinder package (version 2.0.3).

2.7 Data normalization and dimensionality reduction

Gene expression data were normalized using the NormalizeData function in Seurat with the "LogNormalize" method, which scales the expression of each cell by its total expression, multiplies this by a factor of 10,000, and applies a log transformation. Dimensionality reduction was conducted via principal component analysis using the RunPCA function. Cells were clustered based on shared gene expression profiles using the FindClusters algorithm, and were visualized in two dimensions using Uniform Manifold Approximation and Projection (UMAP) via the RunUMAP function.

2.8 Cluster annotation

We used the FindAllMarkers tool in Seurat to annotate cell clusters, employing the default non-parametric Wilcoxon rank sum test with Bonferroni correction. The cell groupings were classified according to differentially expressed genes (DEGs) as well as established cellular markers from the literature. These cell populations included oligodendrocytes (*Plp1* and *Olig1*), endothelial cells (*Itm2a* and *Cldn5*), microglia (*Hexb*), vascular smooth muscle cells (*Acta2* and *Myocd*), astrocytes (*Rorb* and *Aqp4*), neural progenitor cells (*Sox11* and *Dcx*), choroid plexus cells (*Ttr*), pericytes (*Pdgfrb*), macrophages (*Mrc1* and *Cd14*), inhibitory neurons (*Npy*), excitatory neurons (*Snap25* and *Nrg3*), and fibroblast-like cells (*Lum* and *Dcn*).

2.9 Marker gene identification and DEG analysis

To identify differentially expressed genes (DEGs) within each cell type between PKU and control groups, we employed a pseudobulk analysis approach to account for potential pseudo-replication where individual cells are not independent samples. Specifically, UMI counts from cells of the same cell type originating from the same biological replicate (i.e., an individual mouse) were aggregated. This process created a 'pseudobulk' expression profile for each cell type per sample. Subsequently, differential expression analysis was performed on these pseudobulk profiles using the edgeR package. Genes were considered significantly dysregulated at a false discovery rate (FDR) < 0.05 and an absolute log2 (fold-change) > 0.25. For the purpose of cell type annotation, marker genes for each cluster were identified using the FindAllMarkers function with the Presto test in Seurat as a complementary analysis.

2.10 Functional enrichment analysis

Gene Ontology (GO) enrichment analysis (focusing on the Biological Process category) and Kyoto Encyclopedia of Genes and Genomes (KEGG) pathway analysis were performed using the cluster Profiler R package (version 4.6.2). DEGs were input into the enrich GO function for GO analysis and into the enrich KEGG function for KEGG pathway enrichment, using org.Mm.eg.db and KEGG annotation

databases for *Mus musculus*, respectively. All gene IDs were converted to ENTREZ IDs before enrichment. The Benjamini–Hochberg method was used for multiple testing correction, and GO terms or KEGG pathways with a false discovery rate < 0.05 were considered significantly enriched.

2.11 Immunofluorescence Staining and Confocal Microscopy

Mouse brains were dissected and post-fixed in 4% paraformaldehyde (PFA) for 24 hours, followed by cryoprotection in 30% sucrose solution. Coronal sections (30 μm thickness) containing the corpus callosum were prepared using a cryostat. The sections were washed with PBS and blocked for 1 hour at room temperature in a blocking solution containing 0.3% Triton X-100 and 5% normal donkey serum. Subsequently, sections were incubated overnight at 4°C with a primary antibody against Sox10 (rabbit anti-Sox10, Abcam, ab155279, 1:500 dilution). The following day, sections were washed three times with PBS and incubated for 2 hours at room temperature with a fluorescent secondary antibody (donkey anti-rabbit Alexa Fluor 594, Thermo Fisher Scientific, A-11012, 1:1000 dilution). Nuclei were counterstained with DAPI. Images were captured using a laser scanning confocal microscope ([Carl Zeiss LSM880]), and fluorescence intensity was quantified using ImageJ software.

2.12 Statistical analysis

Sample sizes were determined based on established standards for exploratory scRNA-seq studies in rodent models. where (n = 2 ~ 3) biological replicates per group typically suffice to detect major transcriptional shifts across cell types. Specifically, our design (n = 2 ~ 3 mice per group) aligns with protocols for initial discovery-phase brain cell atlases. While no formal power analysis was conducted due to the hypothesis-generating nature of this study, the depth of cellular coverage provides robust resolution for identifying population-level alterations. Data collection and analysis were performed without blinding. All statistical analyses were conducted using R (version 4.2.1) or GraphPad Prism (version 7.04). *P*-values were adjusted for multiple comparisons using the Benjamini–Hochberg method.

3. Results

3.1 Identification of the main cell types in the brain tissue of control and PKU mice

In the present study, to precisely model the genetic etiology of human PKU, we utilized a partially humanized Pah c.1199 + 502A > T knock-in mouse model that our group has previously established and characterized in detail.[9] This model was chosen over the classic, chemically induced Pahenu2 line because the Pahenu2 model carries a missense mutation (p.F263S), whereas our c.1199 + 502A > T model replicates the most prevalent deep-intronic splicing variant found in PKU patients of Asian descent, particularly in China. It faithfully reproduces the splicing defect caused by pseudo-exon inclusion, offering a distinct advantage in genetic fidelity and relevance to the human molecular mechanism. As demonstrated in our previously published phenotypic study, homozygous mice of this

model exhibit a phenotype highly consistent with classical PKU (cPKU), including sustained hyperphenylalaninemia (mean blood PHE > 1200 μmol/L), lower body weight, yellow fur, and marked deficits in spatial learning and memory. These stable characteristics confirm the model's high relevance and reliability for investigating PKU neuropathology.

In the present study, to characterize the cellular landscape of the PKU brain, we generated single-cell suspensions from the brain tissue of 8-week-old PKU and age-matched WT control mice (Fig. 1a). After removing low-quality and doublet cells from the raw scRNA-seq data of two samples per group, dimensionality reduction and clustering identified 24 distinct cell clusters (Fig. 1b and Fig.S1a-c,). Based on canonical marker gene expression, these clusters were annotated and classified into 13 major cell types (Fig. 1c-d, and Table S1). These cell populations included oligodendrocytes (*Plp1* and *Olig1*), endothelial cells (*Itm2a* and *Cldn5*), microglia (*Hexb*), vascular smooth muscle cells (*Acta2* and *Myocd*), astrocytes (*Rorb* and *Aqp4*), neural progenitor cells (*Sox11* and *Dcx*), choroid plexus cells (*Ttr*), pericytes (*Pdgfrb*), macrophages (*Mrc1* and *Cd14*), inhibitory neurons (*Npy*), excitatory neurons (*Snap25* and *Nrg3*), and fibroblast-like cells (*Lum* and *Dcn*) (Fig. 1c).

a, Flowchart of single-cell sequencing of brain tissue. b, The initial clustering of 38,678 single cells derived from mouse brain tissue in the control and PKU groups was visualized using Uniform Manifold Approximation and Projection (UMAP)-based dimensionality reduction. c, Dot plot showing the expression levels of marker genes across 24 clusters. The x-axis represents cell clusters, the y-axis lists marker genes, and the size and color of the dots indicate the percentage of cells expressing the gene and the average expression level, respectively. d, UMAP dimensionality-reduced visualization of major annotated cell types.

3.2 Transcriptional changes in oligodendrocytes

To investigate whether oligodendrocytes exhibit distinct transcriptional programs in PKU, we performed a re-clustering analysis of oligodendrocyte cells. This analysis identified nine distinct cell clusters (C0–C8) (Fig. 2a), thereby enabling the categorization of cells with analogous expression patterns into the same group. The hierarchical clustering dendrogram (Fig. 2b) illustrates the similarities and disparities among the diverse subpopulations (C0–C8) of oligodendrocytes. We then used a stacked bar chart (Fig. 2c) to illustrate and comparatively assess the distributions of cell types across various cell clusters. Regarding oligodendrocytes, PKU group exhibited a pronounced shift in subpopulation composition: clusters C0, C2, C4, C5 and C6 were markedly expanded, whereas clusters C1, C3 and C7 were significantly reduced relative to WT group. To examine the importance of DEGs between the control and PKU groups for oligodendrocytes, we used a volcano plot for their visualization and analysis (Fig. 2d and Table S2), which revealed 334 downregulated genes and 602 upregulated genes. On the basis of these findings, we performed a GO enrichment analysis to investigate the functional associations of the identified DEGs (Fig. 2e). The enriched GO terms were predominantly associated with biological processes such as small GTPase-mediated signal transduction, microtubule organization, neuron axon guidance, axon ensheathment, and actin filament organization. The enhanced categories for cellular components encompassed the extracellular matrix, cell junctions, and the microtubule cytoskeleton.

KEGG pathway enrichment analysis (Fig. 2f) demonstrated significant correlations between DEGs and diverse biological pathways in the control and PKU groups. These pathways encompassed those associated with neurodegenerative diseases—including Huntington's disease, Alzheimer's disease, and Parkinson's disease—in addition to signaling pathways such as cytokine–cytokine receptor interactions and neuroactive ligand–receptor interactions. The enrichment of pathways associated with neurodegenerative diseases suggests that these genes are vital for maintaining the nervous system and for the progression of these conditions. Moreover, the enhancement of signaling channels may indicate alterations in intercellular communication and the regulation of cellular activity.

We then analyzed and quantified the expression levels of several representative DEGs using violin plots to compare the control and PKU groups (Fig. 2g). The expression of genes essential for oligodendrocyte differentiation and myelin sheath function, such as *Sox10* and *Plp1*, was significantly higher in the control group than in the PKU group. Conversely, genes such as *Unc5c* and *Rab31*, were significantly upregulated in the PKU group. These results indicate a complex, bidirectional shift in the transcriptional profile of oligodendrocytes in the PKU state. To further validate the transcriptional findings at the protein level and cellular phenotype, we analyzed *SOX10 +* oligodendrocytes in the corpus callosum using immunofluorescence and quantitative approaches (Fig. 2h). SOX10 is a key transcription factor essential for oligodendrocyte differentiation and maturation. In the immunofluorescence images, *SOX10 +* cells were sparsely distributed in the corpus callosum of the PKU group, whereas they were abundant and densely packed in the WT group. The quantitative analysis of *SOX10 +* cell density in the corpus callosum showed a significant reduction in the PKU group compared to the WT group ($P < 0.05$). This result is consistent with the downregulated expression of *Sox10* at the transcriptional level (Fig. 2g), confirming that PKU impairs the differentiation and maturation of oligodendrocytes in vivo, which may underlie the myelin-related abnormalities and neurodegenerative risks observed in the KEGG and GO enrichment analyses. Collectively, these data demonstrate that PKU induces profound transcriptional and phenotypic alterations in oligodendrocytes, potentially contributing to the neurological deficits associated with this condition.

a, Left panel: UMAP analysis of combined PKU and WT (control) oligodendrocyte single-cell transcriptomes, identifying nine distinct clusters. Right panel: UMAP visualization showing the pronounced separation of oligodendrocyte clusters between the PKU and WT groups. b, Dendrogram illustrating hierarchical clustering relationships among oligodendrocyte clusters (C0–C8). The branching structure reveals the similarity and divergence among different oligodendrocyte subpopulations. c, Stacked bar chart representing the cellular composition of each cluster in both the control and PKU groups. The *y*-axis indicates the percentage of cells within each cluster, whereas the *x*-axis differentiates between the control and PKU conditions. d, V Volcano plot showing differential gene expression between the WT and PKU groups. Genes with downregulated expression in the PKU group are marked in teal, and those with upregulated expression are marked in red. e, Dot plot depicting the enrichment of Gene Ontology (GO) terms in the differentially expressed genes. The *x*-axis represents the GeneRatio, whereas the *y*-axis shows the − log10 (Q value), indicating the significance of enrichment. f, Bar plot illustrating the enrichment of various disease-related pathways in the differentially expressed genes based on Kyoto

Encyclopedia of Genes and Genomes (KEGG) analysis. The *y*-axis lists the pathways, whereas the *x*-axis shows the − log10 (Q value), reflecting the level of enrichment. g, Violin plots comparing the expression levels of selected genes (*Sox10*, *Ptp1*, *Nkx2-2*, *Nfasc*, *Angpt10*, and *Fyn*) between the control and PKU groups. h, Immunofluorescence and quantitative analysis of *SOX10 +* cells in the corpus callosum. Left two panels: Immunofluorescence images of the corpus callosum from PKU and WT groups, with *SOX10 +* cells stained in red and nuclei counterstained in blue. Right panel: Bar graph quantifying the density of *SOX10 +* cells in the corpus callosum of PKU and WT groups.

3.3 Transcriptional changes in astrocytes

To investigate whether astrocytes exhibit distinct transcriptional processes in PKU, we used UMAP to visualize the scRNA-seq data (Fig. 3a). This methodology was chosen to elucidate the similarities and disparities across cell populations between the control and PKU groups. We used a volcano plot for visualization and analysis (Fig. 3b and Table S3) to further examine the relevance of DEGs between the control and PKU groups for astrocytes. Our analysis revealed 80 downregulated genes and 269 upregulated genes. We then conducted GO enrichment analysis to investigate the functional relationships of these DEGs (Fig. 3c). The enriched GO categories were predominantly associated with biological processes, including neural development, cellular signaling, and cell cycle regulation. The enriched categories regarding molecular function comprised protein kinase activity and transcription factor activity. The enriched categories concerning biological components included synapses, cytoplasm, and cell membranes. We then used violin plots to analyze the expression of several representative DEGs (Fig. 3e). The expression of genes related to astrocyte synaptic support and ion homeostasis, such as *Kcnj10* and *Sox9*, was higher in the control group than in the PKU group. In contrast, genes such as *Grm3* and *Ttr* were significantly upregulated in the PKU group, suggesting astrocytes may be in a damage-responsive state. We then constructed a gene interaction network (Fig. 3d) to elucidate the potential linkages and functional associations among important genes identified from single-cell sequencing data of astrocytes from the brain tissue of PKU mice. The network analysis identified *Epha4* as a pivotal hub that had significant interactions with multiple genes, including *Robo2*, *Nrp1*, and *Ephb4*. These interactions are likely implicated in biological processes including cellular signaling, cell adhesion, and cell migration.

a, UMAP plot illustrating the clustering of single-cell samples from PKU and WT groups. b, Volcano plot showing differential gene expression between the WT and PKU groups. Genes with downregulated expression in the PKU group are marked in teal, and those with upregulated expression are marked in red. c, Dot plot depicting the enrichment of GO terms for differentially expressed genes. d, Network diagram representing the interactions between differentially expressed genes and their associated biological pathways. Nodes denote genes or pathways, node size indicates the significance of the gene expression change (log fold change), and the color gradient from green to red illustrates the direction of the fold change. Edges represent relationships between genes and pathways. e, Violin plots presenting the expression levels of selected genes (*Asic2*, *Prkca*, *Dlg5*, *Fgfr2*, *Gpc6*, *Gpm6a, Sox9*, *Hes5*, *Kcnj10*, *Nfix*,

Enpp2, and *Nrros*) across the PKU and WT groups. Each violin plot represents an individual gene, with the distribution summarized by a density plot at the center of each panel.

3.4 Transcriptional changes in microglia

To investigate whether microglia exhibit distinct transcriptional programs in PKU, we used UMAP to visualize the scRNA-seq data (Fig. 4a). To further investigate the importance of DEGs between the control and PKU groups for microglia, we used a volcano plot for visualization and analysis (Fig. 4b and Table S4). Our analysis revealed 229 downregulated genes and 275 upregulated genes. We then performed a GO enrichment analysis to investigate the functional associations of DEGs (Fig. 4c). Microglia were significantly enriched in genes related to oxidative phosphorylation, protein folding, and organic nitrogen compound metabolic activities, implying that these biological processes may be pivotal in the pathogenic progression of PKU. KEGG pathway enrichment analysis indicated that microglia from PKU and control mice are considerably enriched in pathways associated with oxidative phosphorylation, Parkinson's disease, Huntington's disease, and neurodegenerative diseases (Fig. 4d). Consequently, we examined the expression of representative DEGs using violin plots (Fig. 4e). This consistently revealed that numerous genes related to mitochondrial oxidative phosphorylation, such as *Atp5e* and *Ndufb10*, were significantly downregulated in microglia from the PKU group. Conversely, genes such as *Acta2* and *Cox8a* were upregulated in the PKU group. This reflects a complex state of co-existing energy metabolism deficits and immune activation in the PKU brain microenvironment.

a, UMAP plot illustrating the clustering of single-cell samples from PKU and WT groups. b, Volcano plot showing differential gene expression between the WT and PKU groups. Genes with downregulated expression in the PKU group are marked in teal, and those with upregulated expression are marked in red. c, Dot plot depicting the enrichment of GO terms for differentially expressed genes. d, Bar plot illustrating the enrichment of various disease- and pathway-related terms in the differentially expressed genes based on KEGG analysis. e, Violin plots presenting the expression levels of selected genes (*Atp5e, Atp5h, Atp50, Cox7c, Cox7a2, Cox5b, Ndufb5*, *Ndufa13*, *Ndufa2*, *Ndufb10*, *Uqcr10*, and *Uqcr*) across the control and PKU groups.

3.5 Transcriptional changes in endothelial cells

To examine whether endothelial cells display unique transcriptional programs in PKU, we used UMAP to visualize the scRNA-seq data (Fig. 5a). To further examine the relevance of DEGs between the control and PKU groups for endothelial cells, we used a volcano plot for visualization and analysis (Fig. 5b and Table S5). We identified 419 downregulated genes and 877 upregulated genes. Next, we performed a GO enrichment analysis to investigate the functional relationships of DEGs (Fig. 5c). Endothelial cells were markedly enriched in biological activities including intercellular junctions, G protein-coupled receptor signaling, regulation of programmed cell death, and regulation of nervous system development. KEGG pathway enrichment analysis indicated a substantial enrichment in pathways associated with neurodegenerative disorders, proteins, chemical synapses, and cell junctions in microglia from PKU mice compared with those from control mice (Fig. 5d). Subsequently, we examined the expression of

representative DEGs using violin plots (Fig. 5e). The analysis showed that key genes maintaining blood-brain barrier tight junctions and vascular homeostasis, such as *Cldn5* and *Jup*, were downregulated in the PKU group. However, other genes such as *Htr2c* and *Snrk* were significantly upregulated. This may indicate abnormal vascular remodeling or barrier dysfunction in the PKU state.

a, UMAP plot illustrating the clustering of single-cell samples from PKU and WT groups based on their transcriptomic profiles. b, Volcano plot showing differential gene expression between the WT and PKU groups. Genes with downregulated expression in the PKU group are marked in teal, and those with upregulated expression are marked in red. c, Dot plot depicting the enrichment of GO terms for differentially expressed genes. d, Bar plot illustrating the enrichment of various pathways, particularly those related to neurodegeneration, in the differentially expressed genes. e, Violin plots presenting the expression levels of selected genes (*Cldn5*, *Jup*, *Tok*, *Kdr*, *Nrp1*, *Ets1*, *Col4a2*, *Adamts1*, and *Adamts9*) across the control and PKU groups.

4. Discussion

Animal models are crucial in PKU research because they enhance the opportunities for investigating its pathophysiology. Numerous studies using PKU animal models have revealed that elevated PHE levels affect protein synthesis, the transport of large neutral amino acids across the blood–brain barrier, monoamine neurotransmitter production, glutamate receptor activity, and animal behavior.[10]

Our single-cell transcriptomic map provides new molecular links between the core metabolic disturbances in PKU and downstream cellular dysfunctions. A key pathophysiological mechanism is the competition of high circulating phenylalanine with other large neutral amino acids (LNAAs), such as tyrosine and tryptophan, for transport across the blood-brain barrier via transporters like LAT1. This directly limits the availability of precursors for the synthesis of critical monoamine neurotransmitters, including dopamine and serotonin. The dysregulation of neuronal gene expression we observed, particularly those related to synaptic transmission and plasticity, may be a direct transcriptional consequence of this neurotransmitter imbalance. Furthermore, LNAA deficiency and metabolic stress likely trigger broader cellular stress responses. This aligns with our findings of downregulated oxidative phosphorylation pathways in microglia and reduced expression of supportive genes in astrocytes, collectively illustrating how metabolic pressure translates into a coordinated, multi-cell-type dysfunction.

Here, we used scRNA-seq to delineate cell type-specific transcriptional alterations in a mouse model of PKU. Our findings first highlight the coordinated disruption of oligodendrocytes, astrocytes, microglia, and endothelial cells, offering novel insights into the cellular basis of PKU-associated brain dysfunction.

Oligodendrocytes facilitate myelination within the central nervous system. In our analysis, the expression levels of oligodendrocyte-related genes (*Sox10, Plp1*, *Nkx6-2*, *Nasc*, *Arhgef10*, and *Fyn*) were higher in the control group than in the PKU group. To initially validate our findings at the transcriptomic level, we examined Sox10 expression in the corpus callosum of PKU mice using immunofluorescence confocal

microscopy. The results revealed a significant decrease in Sox10 protein levels in PKU mice compared to controls, a finding that is highly consistent with our scRNA-seq data. This further confirms that key regulators of myelination are suppressed in the PKU state.

Sox10 encodes the SRY-box transcription factor 10, a master regulator that orchestrates oligodendrocyte lineage specification and drives the transcription of genes essential for myelin formation.[11] Research indicates that *Sox10* expression facilitates the differentiation of neural crest cells into Schwann cells, oligodendrocytes, and enteric ganglion cells. Moreover, aberrant *Sox10* expression may result in developmental abnormalities of the neurological system, including inadequate myelination and intestinal ganglionitis.[12] *Nkx6-2* encodes the NK6 homeobox 2 transcription factor, which promotes oligodendrocyte maturation and directs axonal ensheathment. Research indicates that *Nkx6-2* is extensively expressed throughout the central nervous system during early development and is crucial for myelin production. The ablation of *Nkx6-2* may result in substantial neurodevelopmental problems, including progressive spastic ataxia and white matter abnormalities.[13] In a murine model, the functional deficiency of *Nkx6-2* is correlated with inadequate myelin formation and impaired motor coordination, mirroring the phenotype seen in humans; this finding suggests that *Nkx6-2* has a unique developmental function in the maturation of neurons and oligodendrocytes.[14] *Fyn* encodes the Src-family tyrosine kinase Fyn, which modulates oligodendrocyte morphology and myelin assembly via cytoskeletal signaling.[15] *Fyn* dysfunction has recently been associated with the pathogenic processes observed in neurodegenerative diseases such as multiple sclerosis, Alzheimer's disease, and Parkinson's disease.[16] Consequently, increased PHE concentrations in PKU may disrupt the myelination process by inhibiting the production of oligodendrocyte-associated genes, thus affecting neuronal conduction and cognitive abilities.

Astrocytes are essential for preserving homeostasis in the central nervous system, regulating redox equilibrium, and influencing synaptic activity. In the present study, the expression levels of genes linked to astrocytes (*Asic2*, *Prkca*, *Dlg5*, *Fgfr2*, *Gpc6*, and *Gpm6a*) were higher in the control group than in the PKU group. *Fgfr2* encodes fibroblast growth factor receptor 2, a receptor tyrosine kinase that controls astrocyte proliferation and regulates dendritic-spine density.[17] *Gpc6* encodes glypican-6, a heparan-sulfate proteoglycan secreted by astrocytes that enhances excitatory synaptogenesis and glutamate-receptor clustering.[18] *Gpm6a* encodes neuronal membrane glycoprotein M6a, which facilitates neurite elongation, axon guidance and synapse formation.[19] In individuals with Alzheimer's disease, *Gpm6a* downregulation in the hippocampus may be associated with changes in neuronal development and synaptic plasticity processes.[20] Sox9 encodes the SRY-box transcription factor 9, a determinant of astrocyte differentiation and neuroprotective gene expression.[18] The diminished expression of these genes may therefore hinder the supportive role of astrocytes for neurons, affect synaptic development and plasticity, and ultimately result in aberrant synaptic control. Consequently, increased PHE concentrations in PKU may impair redox homeostasis and synaptic function by inhibiting the expression of astrocyte-associated genes, thereby altering the normal development and functionality of the nervous system. While human NT2-derived neurons models have identified PHE-induced neurite and synaptic

alterations,[21] our scRNA-seq approach provides unprecedented resolution by mapping transcriptomic dysregulation across all major CNS cell types, including oligodendrocytes, astrocytes, microglia, and endothelial cells, revealing coordinated neuroinflammatory, vascular, and metabolic disruptions that collectively drive PKU neuropathology.

The functions of microglia in energy metabolism and inflammatory polarization are intricately linked, and their operational status is strongly governed by mitochondrial activity. In the present study, the expression levels of genes linked to microglia (*Atp5e*, *Atp5h*, *Atp5o*, *Cox7c*, *Cox7a2*, *Cox5b*, *Ndufb5*, *Ndufa13*, *Ndufa2*, *Ndufb10*, *Uqcr10*, and *Uqcrq*) were higher in the control group than in the PKU group. *Atp5e*, *Atp5h*, and *Atp5o* encode subunits of the mitochondrial ATP synthase complex. The impairment of ATP synthase has frequently been linked to mitochondrial dysfunction, which is a prevalent characteristic of neurodegenerative disorders, and ATP synthase undergoes oxidative changes in conditions such as Alzheimer's, Parkinson's, and Huntington's diseases.[22] These alterations may hinder its normal function, consequently aggravating disease progression.[22] The subunits encoded by *Ndufb5*, *Ndufa13*, *Ndufa2*, and *Ndufb10* are essential constituents of mitochondrial complex I, which contributes to the oxidative phosphorylation process within the cellular respiratory chain and preserves normal mitochondrial function. Mitochondrial dysfunction has an important role in the pathogenesis of PKU. Elevated PHE levels can impair mitochondrial bioenergetics, resulting in oxidative stress and inflammatory reactions.[23] *Uqcrq* encodes ubiquinol-cytochrome c reductase hinge protein 10, a core subunit of mitochondrial respiratory complex III that mediates electron transfer from ubiquinol to cytochrome c and is indispensable for oxidative phosphorylation in microglia.[24] In PKU mice, heightened PHE concentrations may therefore suppress the expression of mitochondria-associated genes in microglia, resulting in compromised energy metabolism and augmented oxidative stress. This may then foster the polarization of microglia toward a pro-inflammatory phenotype, thus intensifying neuroinflammation and neuronal injury.

The expression levels of genes related to endothelial cells (*Cldn5*, *Kdr*, *Nrp1*, *Ets1*, *Col4a2*, *Adamts1*, and *Adamts9*) were higher in the PKU group than in the control group. This finding indicates that endothelial cell function may be aberrantly modified in our mouse model. Nrp1 encodes neuropilin-1, a multifunctional co-receptor for VEGF and semaphorins that modulates vascular guidance and barrier stability. Its overexpression or mutation may result in various anatomical defects in blood vessels, the heart, and the neurological system. [15] Ets1 encodes the E-twenty-six transcription factor 1,[18] a sequence-specific DNA-binding protein that suppresses axonal growth in spinal-cord neurons and down-regulates neural-crest formation through chromatin-remodeling interactions.[25] *Col4a2* encodes the α2 chain of collagen type IV, a basement-membrane component that, when mutated, triggers astrocytic activation and JAK/STAT-mediated neuroinflammation, thereby compromising blood–brain-barrier permeability.[26] In a mouse spinal cord injury model, the expression of a disintegrin and metalloproteinase with thrombospondin motifs 9 (ADAMTS-9) was markedly increased, indicating its essential role in response to central nervous system injury.[27] Consequently, in PKU model animals, increased he concentrations may enhance endothelial cell-associated gene expression, resulting in

aberrant vascular remodeling and the compromised structural and functional integrity of the blood–brain barrier. This might then heighten the susceptibility of the blood–brain barrier and facilitate the onset of neuroinflammation and neuronal injury.

Although our analysis offers a detailed single-cell transcriptome map of PKU-related changes in essential brain cell types, many limitations exist. First, while the partially humanized Pah c.1199 + 502A > T mouse model recapitulates key metabolic and neurological features of human PKU, it remains an imperfect representation of the disease. Species-specific differences in brain development, immune responses, and phenylalanine metabolism may affect translational relevance. Future studies using human iPSC-derived brain organoids or post-mortem PKU patient tissues are required to validate these findings. Second, the investigation was conducted at a single developmental stage (8 weeks of age), and dynamic changes over time have yet to be clarified. Third, the findings of this study are primarily based on transcriptomic data, and their functional consequences require more comprehensive validation. Although our confocal microscopy experiment provides initial confirmation of Sox10 protein downregulation at the tissue level, further experiments, such as direct assessment of myelin changes through immunohistochemistry or electron microscopy, and confirmation of microglial activation states via morphological analysis, remain necessary. Establishing a causal link between these transcriptional changes and cellular pathology is a key direction for future research. The merging of metabolomic and proteomic data may yield more insights into the molecular foundations of PKU. Finally, subsequent research should also investigate how therapeutic approaches, such as tetrahydrobiopterin supplementation or gene therapy, influence these cellular pathways.

5. Conclusions

In conclusion, our single-cell transcriptome analysis indicates that brain of PKU model mouse produces extensive and cell-type-specific transcriptional dysregulation, affecting oligodendrocytes, astrocytes, microglia, and endothelial cells. These modifications hinder myelination, synaptic support, mitochondrial metabolism, and vascular integrity, thereby providing novel insights into the neurodevelopmental impairments associated with PKU and proposing possible treatment targets.

Abbreviations

A Disintegrin and Metalloproteinase With Thrombospondin Motifs 9	ADAMTS-9
Classical PKU	cPKU
Differentially Expressed Genes	DEGs
False Discovery Rate	FDR
Gene Ontology	GO
Kyoto Encyclopedia of Genes and Genomes	KEGG
Large Neutral Amino Acids	LNAAs
Paraformaldehyde	PFA
Phenylalanine	PHE
Phenylalanine Hydroxylase	PAH
Phenylketonuria	PKU
Single-Cell RNA Sequencing	scRNA-seq
Uniform Manifold Approximation and Projection	UMAP
Wild-Type	WT

Declarations

Availability of data and materials

All data generated or analysed during this study are included in this published article and supporting information.

Competing interests

The authors declare that they have no competing interests.

Funding

This research was supported by Beijing Natural Science Foundation (7232062), the Postdoctoral Research Start-up Fund from Beijing Obstetrics and Gynecology Hospital, Capital Medical University; the Postdoctoral Fellowship Program of CPSF (GZC20251416), Gansu Province Joint Research Fund (Grand Number: 25JRRA1236); Major Scientific Research Project for Scientific and Technological Innovation in the Health and Wellness Industry of Gansu Province (Grand Number: GSWSQNPY2025-19).

Author Contributions

YYS and YCH conceived the study; ZC and JXH designed the methodology; ZW and ZHY developed the software; YZY, YHH and HWJ performed validation; CXF carried out formal analysis; CZ conducted investigation; YYS and YCH provided resources; GHM and LWX curated the data and wrote the original draft; GHM and LWX reviewed and edited the manuscript; LWX prepared the visualizations; YYS supervised the project; YYS and YCH administered the project and acquired funding.

Statement for ARRIVE Guidelines Compliance

This study was carried out in accordance with the ARRIVE guidelines (https://arriveguidelines.org). All experimental procedures and reporting adhere to the principles and requirements outlined in the ARRIVE guidelines to ensure the transparency and reproducibility of animal research.

References

1. Hillert A, Anikster Y, Belanger-Quintana A, Burlina A, Burton BK, Carducci C, et al. The genetic landscape and epidemiology of phenylketonuria. Am J Hum Genet. 2020;107(2):234–50.
2. van Spronsen FJ, Blau N, Harding C, Burlina A, Longo N, Bosch AM, Phenylketonuria. Nat Rev Dis Primers. 2021;7(1).
3. Rovelli V, Longo N. Phenylketonuria and the brain. Mol Genet Metab. 2023;139(1).
4. Trepp R, Muri R, Abgottspon S, Bosanska L, Hochuli M, Slotboom J et al. Impact of phenylalanine on cognitive, cerebral, and neurometabolic parameters in adult patients with phenylketonuria (the PICO study): a randomized, placebo-controlled, crossover, noninferiority trial. Trials. 2020;21(1).
5. Bartus A, Palasti F, Juhasz E, Kiss E, Simonova E, Sumanszki C, et al. The influence of blood phenylalanine levels on neurocognitive function in adult PKU patients. Metab Brain Dis. 2018;33(5):1609–15.
6. Bobrova NA, Lyubimova DI, Mishina DM, Lobanova VS, Valieva SI, Mityaeva ON et al. Experimental animal models of phenylketonuria: pros and cons. Int J Mol Sci. 2025;26(11).
7. Bregalda A, Carducci C, Viscomi MT, Pierigè F, Biagiotti S, Menotta M et al. Myelin basic protein recovery during PKU mice lifespan and the potential role of microRNAs on its regulation. Neurobiol Dis. 2023;180.
8. Manek R, Huang W, Huang Y, Guo L, Cornell CS, Shazeeb MS, et al. Blood phenylalanine lowering partially reverses white matter changes in a mouse model of phenylketonuria. Mol Ther. 2025;33(9):4303–19.
9. Zhang C, Yan Y, Zhou B, Gao H, Jin X, Hui L et al. Phenotypic study of humanized mice carrying the PAH deep intronic variant c.1199 + 502A > T. Orphanet J Rare Dis. 2025;20(1).
10. Rausell D, García-Blanco A, Correcher P, Vitoria I, Vento M, Cháfer-Pericás C. Newly validated biomarkers of brain damage may shed light into the role of oxidative stress in the pathophysiology of neurocognitive impairment in dietary restricted phenylketonuria patients. Pediatr Res. 2019;85(2):242–50.

11. Kidwai F, Mui BWH, Arora D, Iqbal K, Hockaday M, de Castro Diaz LF, et al. Lineage-specific differentiation of osteogenic progenitors from pluripotent stem cells reveals the FGF1-RUNX2 association in neural crest-derived osteoprogenitors. Stem Cells. 2020;38(9):1107–23.
12. Bhattarai C, Poudel PP, Ghosh A, Kalthur SG. Comparative role of SOX10 gene in the gliogenesis of central, peripheral, and enteric nervous systems. Differentiation. 2022;128:13–25.
13. Baldi C, Bertoli-Avella AM, Al-Sannaa N, Alfadhel M, Al-Thihli K, Alameer S, et al. Expanding the clinical and genetic spectra of NKX6-2-related disorder. Clin Genet. 2018;93(5):1087–92.
14. Chelban V, Patel N, Vandrovcova J, Zanetti MN, Lynch DS, Ryten M, et al. Mutations in NKX6-2 cause progressive spastic ataxia and hypomyelination. Am J Hum Genet. 2017;100(6):969–77.
15. Brown TL, Hashimoto H, Finseth LT, Wood TL, Macklin WB. PAK1 positively regulates oligodendrocyte morphology and myelination. J Neurosci. 2021;41(9):1864–77.
16. Guglietti B, Sivasankar S, Mustafa S, Corrigan F, Collins-Praino LE. Fyn kinase activity and its role in neurodegenerative disease pathology: a potential universal target? Mol Neurobiol. 2021;58(11):5986–6005.
17. Szczurkowska J, Pischedda F, Pinto B, Managò F, Haas CA, Summa M et al. NEGR1 and FGFR2 cooperatively regulate cortical development and core behaviours related to autism disorders in mice. Brain. 2018.
18. Allen NJ, Bennett ML, Foo LC, Wang GX, Chakraborty C, Smith SJ, et al. Astrocyte glypicans 4 and 6 promote formation of excitatory synapses via GluA1 AMPA receptors. Nature. 2012;486(7403):410–4.
19. Gutiérrez Fuster R, León A, Aparicio GI, Brizuela Sotelo F, Scorticati C. Combined additive effects of neuronal membrane glycoprotein GPM6a and the intercellular cell adhesion molecule ICAM5 on neuronal morphogenesis. J Neurochem. 2024;169(1).
20. León A, Sallaberry I, Fuster RG, Sotelo FB, Aparicio GI, Estrada LC et al. Non-synonymous single nucleotide polymorphisms (nsSNPs) within the extracellular domains of the GPM6A gene impair hippocampal neuron development. BBA-Mol Cell Res. 2025;1872(3).
21. Stankovic S, Lazic A, Parezanovic M, Stevanovic M, Pavlovic S, Stojiljkovic M et al. Transcriptome profiling of phenylalanine-treated human neuronal model: spotlight on neurite impairment and synaptic connectivity. Int J Mol Sci. 2024;25(18).
22. Ebanks B, Chakrabarti L. Mitochondrial ATP synthase is a target of oxidative stress in neurodegenerative diseases. Front Mol Biosci. 2022;9.
23. Wyse ATS, dos Santos TM, Seminotti B, Leipnitz G. Insights from animal models on the pathophysiology of hyperphenylalaninemia: role of mitochondrial dysfunction, oxidative stress and inflammation. Mol Neurobiol. 2021;58(6):2897–909.
24. Hung Y-C, Huang K-L, Chen P-L, Li J-L, Lu SH-A, Chang J-C et al. UQCRC1 engages cytochrome c for neuronal apoptotic cell death. Cell Rep. 2021;36(12).
25. Blau N. Genetics of phenylketonuria: then and now. Hum Mutat. 2016;37(6):508–15.

26. Hu C, Liu D, Wang H. Col4a2 mutations contribute to infantile epileptic spasm syndrome and neuroinflammation. Int J Med Sci. 2024;21(9):1756–68.
27. Demircan K, Yonezawa T, Takigawa T, Topcu V, Erdogan S, Ucar F, et al. ADAMTS1, ADAMTS5, ADAMTS9 and aggrecanase-generated proteoglycan fragments are induced following spinal cord injury in mouse. Neurosc Lett. 2013;544:25–30.

Figures

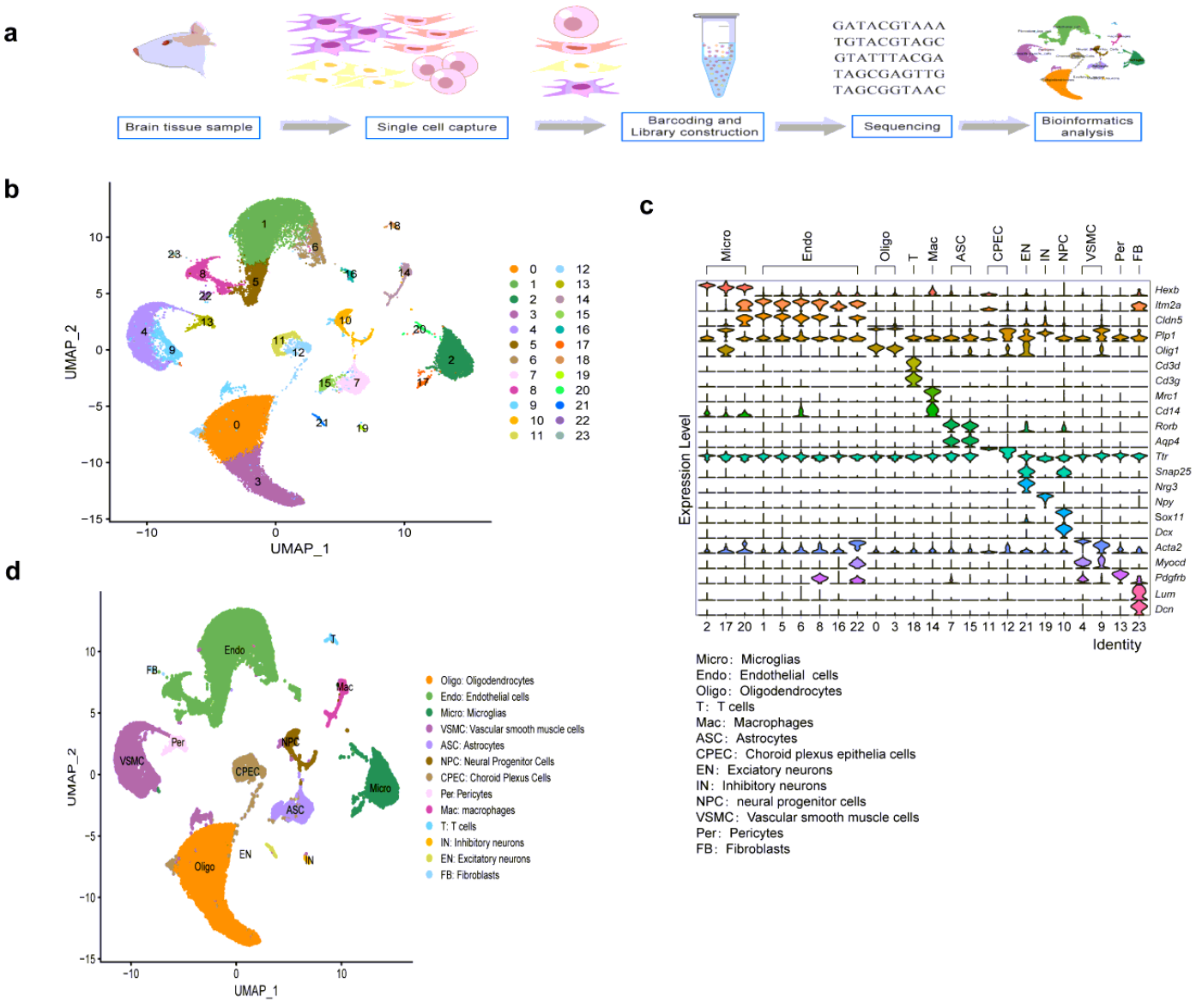


Figure 1

Single-cell clustering and annotation of brain tissue from wild-type (WT) and phenylketonuria (PKU) mice.

a, Flowchart of single-cell sequencing of brain tissue. b, The initial clustering of 38,678 single cells derived from mouse brain tissue in the control and PKU groups was visualized using Uniform Manifold Approximation and Projection (UMAP)-based dimensionality reduction. c, Dot plot showing the expression levels of marker genes across 24 clusters. The x-axis represents cell clusters, the y-axis lists marker genes, and the size and color of the dots indicate the percentage of cells expressing the gene and the average expression level, respectively. d, UMAP dimensionality-reduced visualization of major annotated cell types.

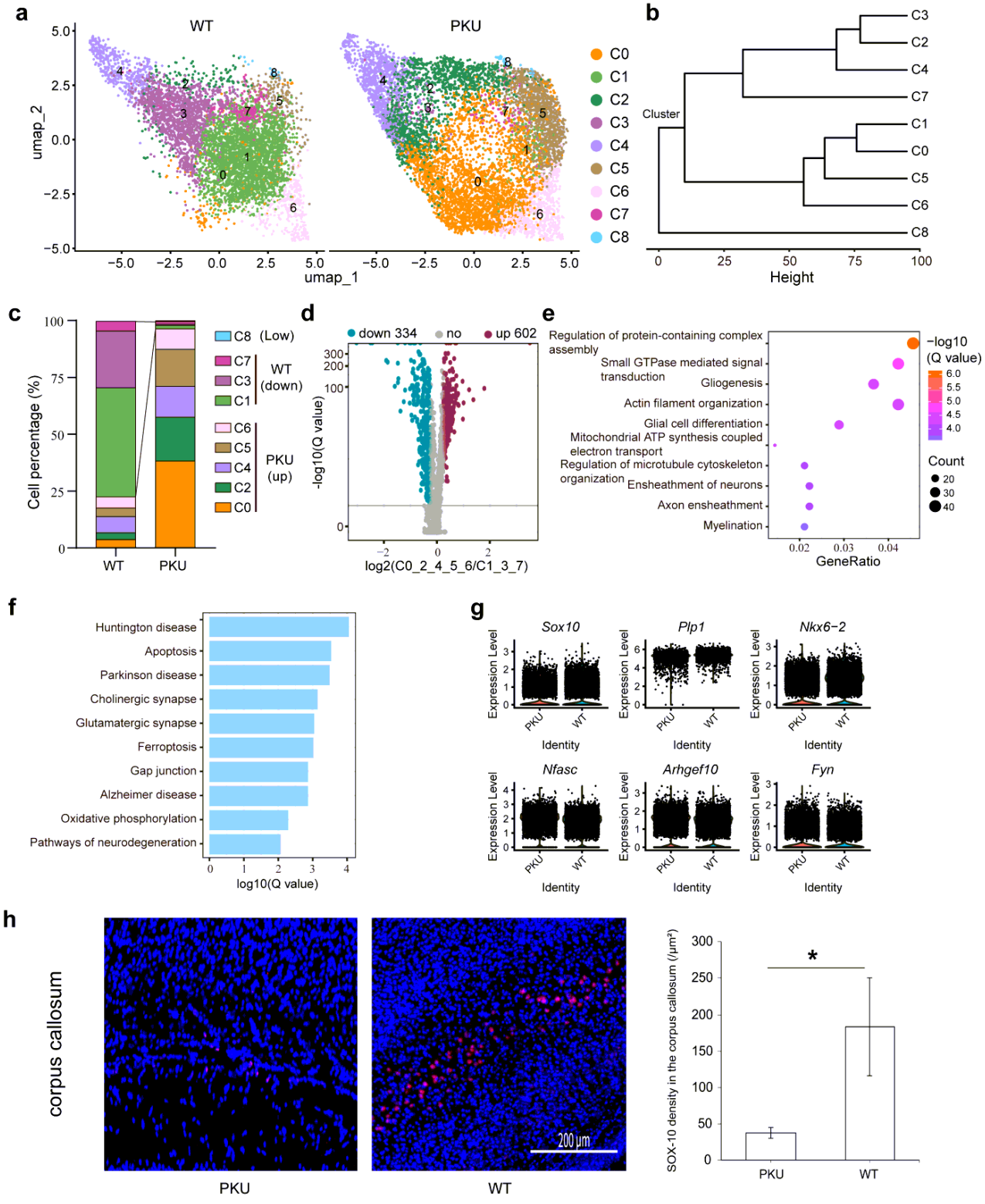


Figure 2

Oligodendrocytes in PKU mice exhibit altered transcriptional states compared with those in WT mice.

a, Left panel: UMAP analysis of combined PKU and WT (control) oligodendrocyte single-cell transcriptomes, identifying nine distinct clusters. Right panel: UMAP visualization showing the pronounced separation of oligodendrocyte clusters between the PKU and WT groups. b, Dendrogram illustrating hierarchical clustering relationships among oligodendrocyte clusters (C0–C8). The branching structure reveals the similarity and divergence among different oligodendrocyte subpopulations. c, Stacked bar chart representing the cellular composition of each cluster in both the control and PKU groups. The *y*-axis indicates the percentage of cells within each cluster, whereas the *x*-axis differentiates between the control and PKU conditions. d, V Volcano plot showing differential gene expression between the WT and PKU groups. Genes with downregulated expression in the PKU group are marked in teal, and those with upregulated expression are marked in red. e, Dot plot depicting the enrichment of Gene Ontology (GO) terms in the differentially expressed genes. The *x*-axis represents the GeneRatio, whereas the *y*-axis shows the −log10 (Q value), indicating the significance of enrichment. f, Bar plot illustrating the enrichment of various disease-related pathways in the differentially expressed genes based on Kyoto Encyclopedia of Genes and Genomes (KEGG) analysis. The *y*-axis lists the pathways, whereas the *x*-axis shows the −log10 (Q value), reflecting the level of enrichment. g, Violin plots comparing the expression levels of selected genes (*Sox10*, *Ptp1*, *Nkx2-2*, *Nfasc*,*Angpt10*, and *Fyn*) between the control and PKU groups. h, Immunofluorescence and quantitative analysis of *SOX10+* cells in the corpus callosum. Left two panels: Immunofluorescence images of the corpus callosum from PKU and WT groups, with *SOX10+* cells stained in red and nuclei counterstained in blue. Right panel: Bar graph quantifying the density of *SOX10+* cells in the corpus callosum of PKU and WT groups.

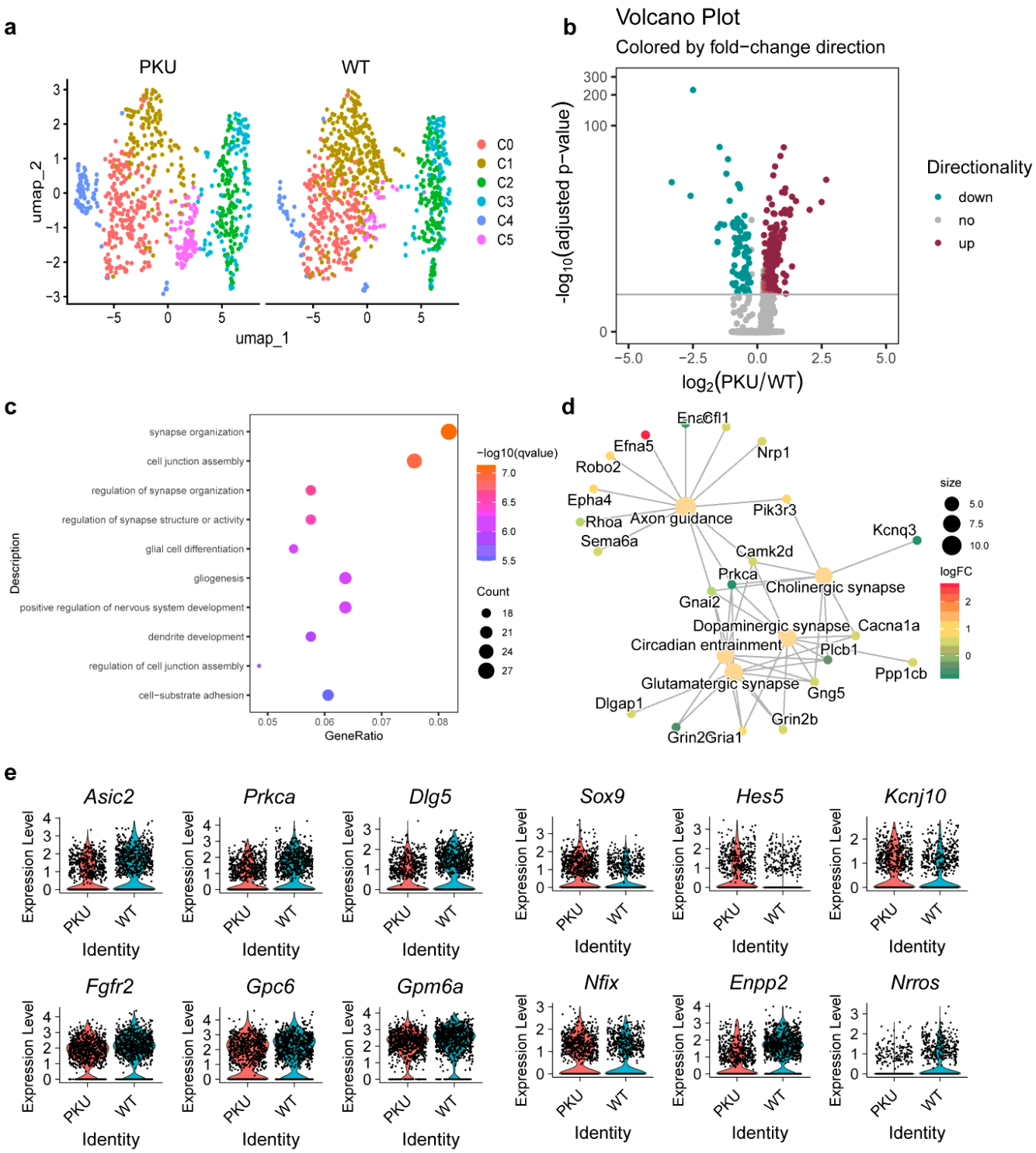


Figure 3

Astrocytes in PKU mice exhibit altered transcriptional states compared with those in WT mice.

a, UMAP plot illustrating the clustering of single-cell samples from PKU and WT groups. b, Volcano plot showing differential gene expression between the WT and PKU groups. Genes with downregulated expression in the PKU group are marked in teal, and those with upregulated expression are marked in

red. c, Dot plot depicting the enrichment of GO terms for differentially expressed genes. d, Network diagram representing the interactions between differentially expressed genes and their associated biological pathways. Nodes denote genes or pathways, node size indicates the significance of the gene expression change (log fold change), and the color gradient from green to red illustrates the direction of the fold change. Edges represent relationships between genes and pathways. e, Violin plots presenting the expression levels of selected genes (*Asic2*,*Prkca*, *Dlg5*, *Fgfr2*, *Gpc6*, *Gpm6a, Sox9*, *Hes5*,*Kcnj10*, *Nfix*, *Enpp2*, and *Nrros*) across the PKU and WT groups. Each violin plot represents an individual gene, with the distribution summarized by a density plot at the center of each panel.

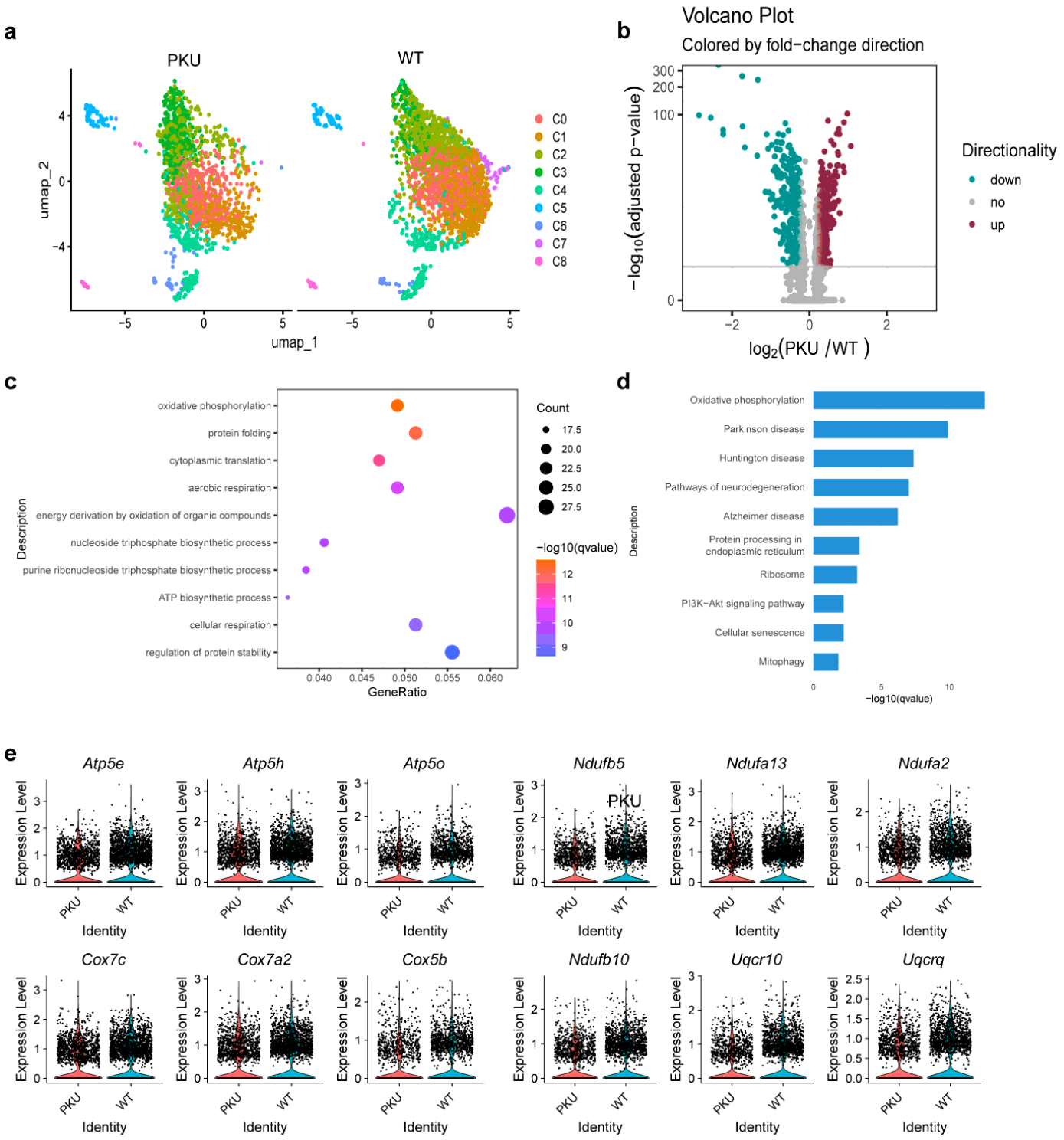


Figure 4

Microglia in PKU mice exhibit altered transcriptional states compared with those in WT mice.

a, UMAP plot illustrating the clustering of single-cell samples from PKU and WT groups. b, Volcano plot showing differential gene expression between the WT and PKU groups. Genes with downregulated expression in the PKU group are marked in teal, and those with upregulated expression are marked in

red. c, Dot plot depicting the enrichment of GO terms for differentially expressed genes. d, Bar plot illustrating the enrichment of various disease- and pathway-related terms in the differentially expressed genes based on KEGG analysis. e, Violin plots presenting the expression levels of selected genes (*Atp5e, Atp5h, Atp50, Cox7c, Cox7a2, Cox5b, Ndufb5*, *Ndufa13*, *Ndufa2*, *Ndufb10*,*Uqcr10*, and *Uqcr*) across the control and PKU groups.

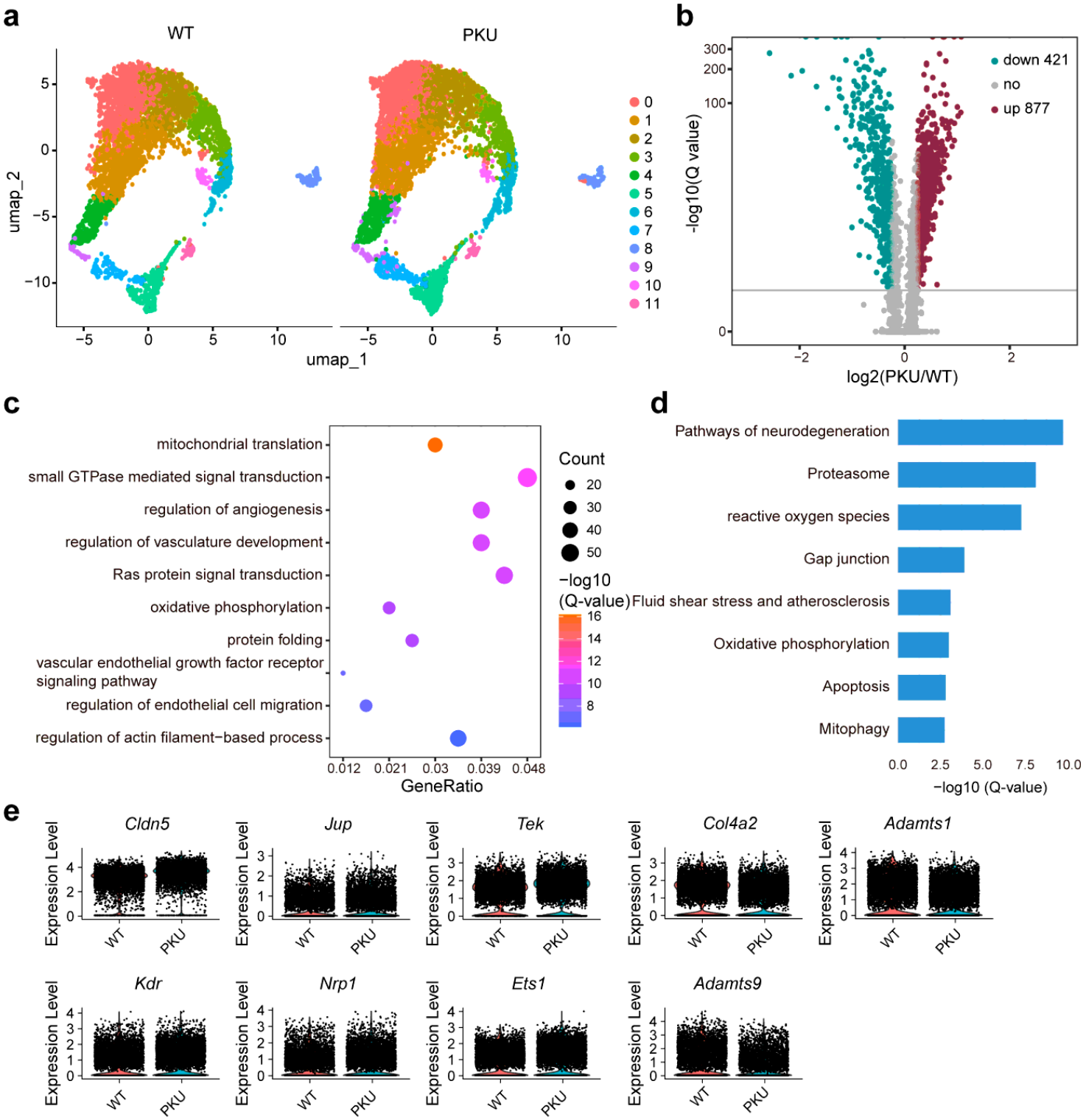


Figure 5

Endothelial cells in PKU mice exhibit altered transcriptional states compared with those in WT mice.

a, UMAP plot illustrating the clustering of single-cell samples from PKU and WT groups based on their transcriptomic profiles. b, Volcano plot showing differential gene expression between the WT and PKU groups. Genes with downregulated expression in the PKU group are marked in teal, and those with upregulated expression are marked in red. c, Dot plot depicting the enrichment of GO terms for differentially expressed genes. d, Bar plot illustrating the enrichment of various pathways, particularly those related to neurodegeneration, in the differentially expressed genes. e, Violin plots presenting the expression levels of selected genes (*Cldn5*, *Jup*, *Tok*, *Kdr*,*Nrp1*, *Ets1*, *Col4a2*, *Adamts1*, and *Adamts9*) across the control and PKU groups.

Supplementary Files

This is a list of supplementary files associated with this preprint. Click to download.

- FigS1.docx
- Supportinginformation.docx
- TableS1..csv
- TableS2..csv
- TableS3..csv
- TableS4..csv
- TableS5..csv